ELSEVIER

Polymer 42 (2001) 8249–8264

polymer

www.elsevier.nl/locate/polymer

The structure and properties of cellulose fibres spun from an anisotropic phosphoric acid solution

M.G. Northolt*, H. Boerstoel, H. Maatman, R. Huisman, J. Veurink, H. Elzerman

Acordis Research, P.O. Box 9600, 6800 TC Arnhem, The Netherlands

Received 18 January 2001; received in revised form 8 March 2001; accepted 14 March 2001

Abstract

The structure and the mechanical properties of a newly developed highmodulus/high strength cellulose fibre spun from an anisotropic solution in phosphoric acid are discussed and compared with those of existing regenerated cellulose fibres. The crystal structure of the fibre is of the cellulose II modification, and the highly oriented and crystalline fibres have an initial filament modulus of 44 GPa, a sonic modulus of 58 GPa, and a strength of 1.7 GPa. It is shown that the mechanical properties of this fibre are well described by the continuous chain model. Lateral birefringence measurements and an electron diffraction study have established the orientation of the optical axes n_α and n_β relative to the *a* and *b* axes in the crystal structure. Moreover, the most likely crack directions in the cellulose II structure have been identified.

Keywords: Cellulose; Fibre; Structure; Mechanical properties

1. Introduction

Regenerated cellulose fibres have long been made according to various processes yielding fibres with a wide range of mechanical properties. They include textile fibres with a low modulus and tenacity but high elongation at break, fibres for technical applications such as tire yarns with an intermediate modulus and strength, and fibres with a high modulus and tenacity but low elongation at break [1–5].

In the present paper, we report on the structure and mechanical properties of a highly oriented cellulose fibre spun from an anisotropic solution in phosphoric acid using an air gap [6]. A number of processes have been developed for the commercial production of cellulose yarns, both for textile and industrial applications. Yarns of these processes all have a limited tenacity. Among them are those made by the viscose, cuprammmonium, Fortisan® and *N*-methyl morpholine oxide (NMMO) processes [7]. Yarns made by the last three processes are not commercially available any more. Two processes from the patent literature have demonstrated the great potential of cellulose in making high tenacity, high modulus yarns. In the viscose process, cellulose xanthate (Cell–O–CS_2Na) is dissolved in an alkali solution and spun into a coagulation bath of diluted sulfuric acid, during which stretching is applied, the stretch ratio depending on the desired properties of the yarn. These yarns — referred to as Enka® Viscose and Cordenka® — serve textile and industrial applications, respectively. A high modulus variant is Cordenka® EHM, now out of production, which was made by adding formaldehyde either to the spinning bath or the spinning dope. This slows down coagulation, as a consequence of which the yarn could be stretched further [2]. In the cuprammonium process, cellulose is dissolved in a mixture of copper sulfate and ammoniumhydroxide. In 1931, the possibility of spinning this solution via an air gap was already claimed in a Bemberg patent [8]. Fortisan® is a saponified cellulose acetate, which is prepared by dry spinning from a solution of cellulose acetate in acetone. Use is made of the thermoplastic properties of cellulose acetate by stretching in steam under pressure in order to improve orientation. Subsequently, the cellulose acetate is saponified in caustic soda or sodium acetate [5,9]. In the NMMO-process, cellulose and an aqueous NMMO-solution are mixed to form a slurry. Water is then evaporated and the cellulose starts to dissolve. As an explosive mixture can be formed, the solution is stabilized by adding propyl gallate [10–12]. The solution is spun through an air gap, in which stretching is applied, into an aqueous coagulation bath. Courtaulds has commercialized the process for staple fibre production (Tencel®), while Akzo Nobel operates a pilot plant for filament yarns

* Corresponding author. Tel.: +31-26-3664056; fax: +31-26-3663009.
E-mail address: maurits.northolt@research-ahm.acordis.com (M.G. Northolt).

0032-3861/01/$ - see front matter
PII: S0032-3861(01)00211-7

(NewCell®) and Lenzing for staple fibres (Lenzing® Lyocell). In patent applications by DuPont the preparation of high tenacity filaments is described [13,14]. Cellulose acetate is dissolved in trifluoroacetic acid, to form a liquid crystalline solution, which is spun via an air gap into a methanol coagulation bath. The cellulose acetate fibre is optionally stretched in steam to improve orientation and then saponified with an alkali solution. The patent mentions filament tenacities of 2.7 GPa for a test length of one inch for a number of filaments, which indicates the high potential when a yarn is produced from an anisotropic cellulose solution. A Michelin patent application describes another process for making high tenacity cellulose yarns [15]. Cellulose is dissolved in a mixture of formic acid and phosphoric acid. In situ derivatization occurs, as a consequence of which cellulose formate is formed, which dissolves in phosphoric acid and the excess amount of formic acid. The resulting liquid crystalline solution is spun through an air gap, in which stretching is applied, into an acetone coagulation bath. Subsequently, the cellulose formate yarn is saponified.

Liquid crystalline solutions are known to be good precursors for high modulus/high tenacity yarns. The backbones of most of the polymers used for the preparation of these strong fibres comprise aromatic units, e.g. poly(*p*-phenylene terephthalamide) or PpPTA, polybenzoxazole or PBO, polybenzothiazole or PBT, and recently poly{2,6-di-imidazo [4,5-b:4′5′-e]pyridinylene-1,4-(2,5-dihydroxy)phenylene} or PIPD, but as already mentioned cellulose derivatives have also been used [16,17]. The advantage of using a liquid crystalline solution for fibre production is that the local orientational order of the chains is already at such a level that they can be transformed into highly oriented fibres without the necessity of an after-treatment, which is required in spinning from isotropic melts or solutions of flexible polymers [18]. Reviews of mesophases of cellulose-based polymers have been presented by Gray and Gilbert [19–21]. We divide the systems into those based on derivatized and nonderivatized cellulose. Hydroxypropyl cellulose in water was the first cellulose derivative for which a mesophase was reported [22]. After this first publication the system has been studied extensively and many more mesophases of solutions of cellulose derivatives in a great number of solvents have been described [19–21]. Cellulose esters and ethers form mesophases in both organic solvents and inorganic acids [23–25]. As already mentioned, a liquid crystalline solution of cellulose acetate in, e.g. trifluoroacetic acid has been used to spin highly oriented fibres [13,14]. The same holds for anisotropic solutions of cellulose formate in a mixture of formic acid and phosphoric acid [15]. Mesophases of nonderivatized cellulose are scarce. Reports on anisotropic solutions of cellulose have been given for NMMO/water [26,27], trifluoroacetic acid/dichloromethane [28], DMAc/LiCl [29–32], ammonia/ammonium thiocyanate [33,34], and a specific mixture of one part sulfuric acid (SA), eight parts polyphosphoric acid (PPA), and one part water [35,36].

Allthough isotropic solutions of cellulose in phosphoric acid have long been known, it was only recently discovered that anisotropic solutions can also be formed [6,37–39]. Until then it was assume that either cellulose had to be derivatized, or that a cosolvent as sulfuric acid was needed to form anisotropic solutions in phosphoric acid [15,24,25,35]. The cosolvent was said to form a complex with polyphosphoric acid. This complex was considered to account for the occurrence of an anisotropic phase. Surprisingly, it was found that neither substitution nor a cosolvent is required for the formation of anisotropic solutions in phosphoric acid [6]. It was observed that optimum results were obtained under waterfree conditions. It follows that orthophosphoric acid as such is not very suitable, because of the presence of a certain amount of water.

Phosphoric acid is a special acid in that it can form dimers, oligomers and even polymeric forms. Orthophosphoric acid can be considered as the reaction product of phosphorus pentoxide and water; pyrophosphoric acid ($H_4P_2O_7$) is the dimer of orthophosphoric acid. Polyphosphoric acid as used in the work as described in this paper has the overall composition of $H_6P_4O_{13}$. The compositions can all be characterized in terms of their P_2O_5-concentration. Consequently, orthophosphoric acid corresponds to a P_2O_5-content of 72.4%, pyrophosphoric acid of 79.6% and polyphosphoric acid ($H_6P_4O_{13}$) of 84%. In the P_2O_5–water system, there is always a distribution of the various kinds of phosphoric acids, the equilibrium of which depends on the composition [40,41].

It was found that water has a detrimental effect on the anisotropic properties of the solution, as shown by a decrease of the clearing temperature. This may be caused by a competition between water and the hydroxyls of cellulose in the interaction with phosphoric acid [42]. Water free conditions are reached for concentrations equal or larger than the composition of orthophosphoric acid; these higher concentrations can be obtained by mixing two or more of the following components: orthophosphoric acid, pyrophosphoric acid, polyphosphoric acid, phosphorus pentoxide, and water. It may take a considerable time before the new equilibrium distribution of the acids is reached, especially if the starting composition is much different from this new equilibrium distribution. Although in a wider range anisotropy was found, the optimum results were obtained when the P_2O_5-concentration of the solvent lies in between 72 and 76% w/w. In this range, the melting temperature of the solvent is below room temperature. However, phosphoric acid can be supercooled, and in this process it is often used in a metastable state.

Cellulose rapidly dissolves in the phosphoric acid mixture, and the solutions are already anisotropic above a polymer concentration of 8% w/w, which is extremely low, taking into account the semiflexible nature of the cellulose chain. This critical concentration is even comparable to the one for a polymer as rigid as PpPTA in sulfuric acid [18]. Therefore, this cellulose solution is

eminently suited for the production of high modulus/high tenacity yarns.

2. Structure and mechanical properties of cellulose fibres

The investigation of the relation between the structure and mechanical properties of regenerated cellulose fibres has stimulated the development of the polymer fibres in general. Important contributions have been made by, among others, Meyer and Lotmar, Baule and Kratky, Ingersoll, Hermans, de Vries, Kast, Kiessig, Sprague and Noether [5,43–51]. In terms of morphology and microstructure, the regenerated cellulose fibres can be positioned in between the semicrystalline fibres with the two-phase structure of amorphous and crystalline domains, such as the aliphatic polyamides and the polyesters, and the single-phase paracrystalline structure of fibres made from rigid-rod polymer chains such as the PpPTA, PBO and PBT [16]. A number of cellulose derivatives showing mesophase formation appear to have a persistence length ranging from 6 to 11 nm [52]. A theoretical estimate for the persistence length of the cellulose chain in water yields about 14 nm [53]. Because of the wet spinning process the cellulose fibres show a structure and morphology that have many features in common with those found in the rigid-rod fibres [54]. As shown in this study, this similarity is enhanced when cellulose fibres are spun from an anisotropic solution applying an air-gap, i.e. in a process, which strongly resembles that applied for the (well-known) rigid-rod polymers PpPTA and PBO. In this respect, it is striking that cellulose fibres, like aramid and PBO fibres, do not show a meridional small-angle X-ray diffraction peak characteristic for a two-phase structure consisting of a series arrangement of crystalline and less dense amorphous domains. Only after heating cellulose fibres in water at 200°C or treating the fibres for 100 h with a dilute hydrogenchloride solution will a weak meridional peak appear. This has led Kiessig to conclude that the crystalline domains in cellulose fibres are separated by domains which are somewhat less ordered but certainly not amorphous, as in the aliphatic polyamides and polyesters [51]. All these wet spun fibres, however, do show a continuous equatorial scattering pattern, indicating an elongated fibrillar structure parallel to the fibre axis. As will be shown, the paracrystalline structure of the new cellulose fibre results in mechanical properties which, when normalized by the chain modulus, are quite similar to those obtained for the high-modulus and high-strength PpPTA and PBO fibres.

The cellulose chain can adopt two conformations. In the cellulose I form there are two intramolecular hydrogen bonds between the successive anhydroglucose units, O(2)···O(6) and (O3)···O(5), whereas in the cellulose II form only a bifurcated intramolecular hydrogen bond (O(3)···O(5),O(6)) is found parallel to the ether bridge as shown in Fig. 1. The formation of these intramolecular hydrogen bonds depends on the conformation of the hydroxymethyl group, which adopts the *trans–gauche* (*tg*) conformation in the cellulose I chain and the *gt* conformation in the chain with only the bifurcated hydrogen bond [55]. Cellulose I is only found in natural fibres, i.e. in a rather pure fibre form in flax, manila, ramie and sisal, whereas the cellulose II form is only observed in regenerated fibres. The two different conformations of the hydroxymethyl group that cause the difference in intramolecular hydrogen bonding have important consequences for the ultimate tensile properties of the fibres. The modulus of the celluose I chain is 140 GPa and that of cellulose II only 90 GPa [55,56]. This difference explains how it is that dynamic tensile moduli have been found for some native cellulose fibres with values in excess of 80 GPa and up to nearly 120 GPa just before rupture, whereas the dynamic modulus for highly oriented regenerated cellulose fibres shortly before rupture does not exceed 60 GPa [57].

The tensile properties of polymer fibres are well understood on the basis of the continuous chain model, which is a further development of the series or uniform stress model [58–60]. The fibre is considered to be composed of a serial arrangement of small domains. In a domain the chains are oriented parallel to the symmetry axis and the orientation angle of this axis ϕ with the fibre axis follows a distribution $\rho(\phi)$. The extension of the fibre is calculated from the changes of the projected length of the polymer chain. The continuous chain model shows that the elastic tensile deformation is due to the combined effect of the elongation of the polymer chain and the shear deformation of a small domain containing the chain segment. The shear deformation induces a rotation of the direction of the chain segment towards the fibre axis [60–62]. According to this model the initial tensile modulus of a fibre is

$$\frac{1}{E} = \frac{1}{e_c} + \frac{\langle \sin^2 \phi_0 \rangle_E}{2g}\left[1 - \frac{2g(1+\nu_{13})}{e_c}\right]. \quad (1)$$

Here e_c is the chain modulus (for cellulose II equal to 90 GPa), g the average modulus for shear between adjacent chains, ν_{13} Poisson's ratio and $\langle \sin^2 \phi_0 \rangle_E$ the strain orientation parameter at zero load, the average being taken over the whole orientation distribution of the chains. The birefringence of the fibre given by

$$\frac{\Delta n}{\Delta n_{max}} = 1 - \frac{3}{2}\langle \sin^2 \phi_0 \rangle \quad (2)$$

with Δn_{max} being the maximum value of the birefringence, yields the conventional orientation parameter $\langle \sin^2 \phi_0 \rangle$, which is obtained by averaging over all the chains in the crystalline and in the less ordered domains [61,63]. From the azimuthal distribution of a meridional or an equatorial reflection in the fibres X-ray diffraction pattern only the orientation distribution of the chains in the crystalline domains can be derived.

Thus high-modulus fibres are obtained by maximizing the

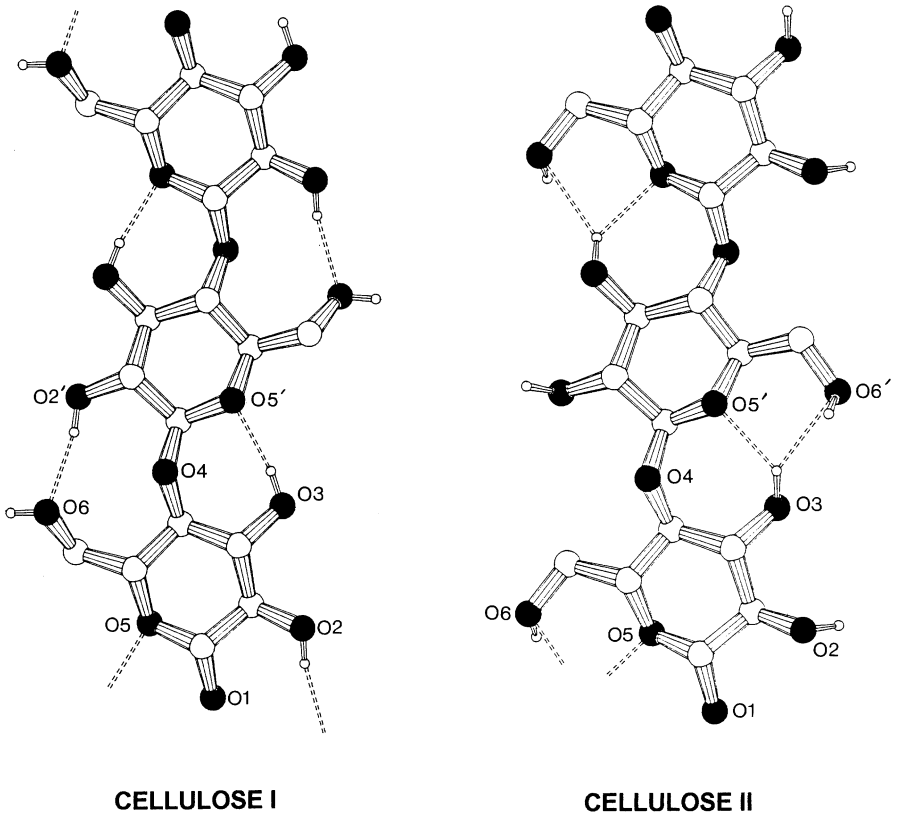

Fig. 1. The chain conformations of cellulose I (left) and celluose II (right).

parallel orientation of the chains, and by the same token minimizing the orientation parameters $\langle \sin^2 \phi_0 \rangle$ and $\langle \sin^{2-} \phi_0 \rangle_E$. Due to the van der Waals and hydrogen bonds between the chains the shear modulus g is frequency or time dependent, while the chain modulus is a purely elastic property. In cellulose II fibres the value of g is to a large extent determined by the intermolecular hydrogen bonding. Fig. 2 shows the different modes of chain packing in the two cellulose crystal modifications as viewed along the chain axis [64–66]. In cellulose I, the hydrogen bonds are formed between adjacent chains in 010 planes which are linked by van der Waals bonds, whereas in cellulose II each chain is hydrogen bonded to four of its neighbours. Similar uni- and bidirectional hydrogen-bonding is found in the crystal structures of poly(*p*-phenylene terephthalamide) and poly(*m*-phenylene terephthalamide), respectively [67–69]. This difference in the lateral hydrogen bonding is likely to be the cause of the different values of the shear modulus, g, for cellulose I and rayon fibres, viz. 1.5 and 2.5 GPa, respectively [57].

The average shear modulus g can be determined from the tensile modulus and the strain orientation parameter by using Eq. (1). According to the continuous chain model the contributions to the fibre extension are the elastic elongation of the chain and the rotation of the chain towards the fibre axis due to shear. This shear deformation, which has an elastic, a viscoelastic, and a plastic component, results in a contraction of the chain orientation distribution during extension of the fibre. Now a relation can be derived between the change in the sonic compliance, $S = E^{-1}$, and the corresponding change of the shear contribution, ϵ_{rot}, to the strain, which in its simplest form can be represented by

$$g \approx \frac{\Delta \epsilon_{\text{rot}}}{\Delta S}. \tag{3}$$

The shear contribution to the strain is defined by

$$\epsilon_{\text{rot}} = \frac{\langle \cos\phi \rangle - \langle \cos\phi_0 \rangle}{\langle \cos\phi_0 \rangle} = \epsilon_{\text{f}} - \frac{\sigma_f}{e_c}. \tag{4}$$

σ_{f} and ϵ_{f} being the fibre stress and strain, respectively. So the shear modulus at sonic frequencies can be determined from the measurement of the sonic modulus during tensile extension of the fibre [59,60]. Because during first loading of a fibre parallel slip of chains may occur, yielding a contribution to the strain not related to chain rotation, the shear modulus is determined from curves measured during unloading of the fibre.

A decrease in the perfectness of the chain orientation in non-flexible chain polymers causes a decrease in lateral order, and hence in a lower crystallinity. As a result of the lower crystallinity the average distance between the chains is increased, thereby reducing the interchain bonding and

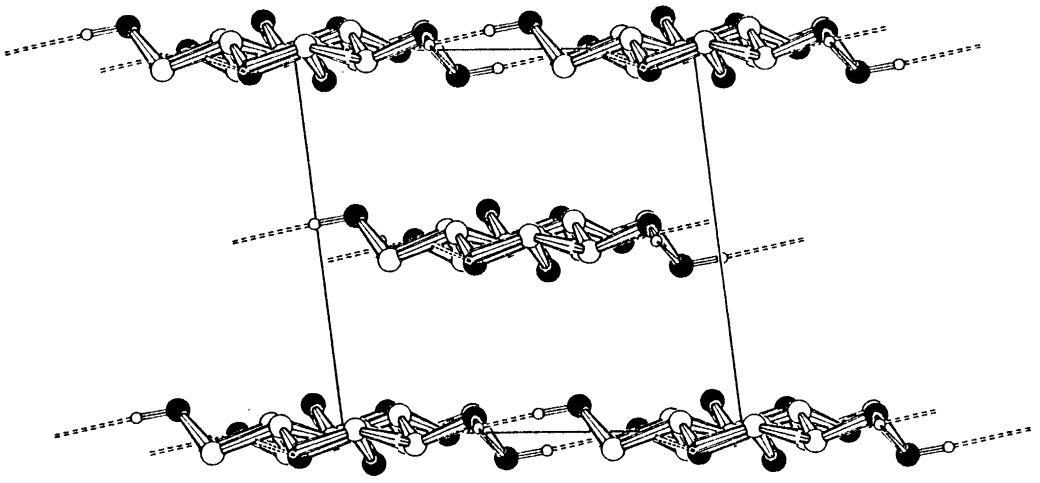

CELLULOSE I

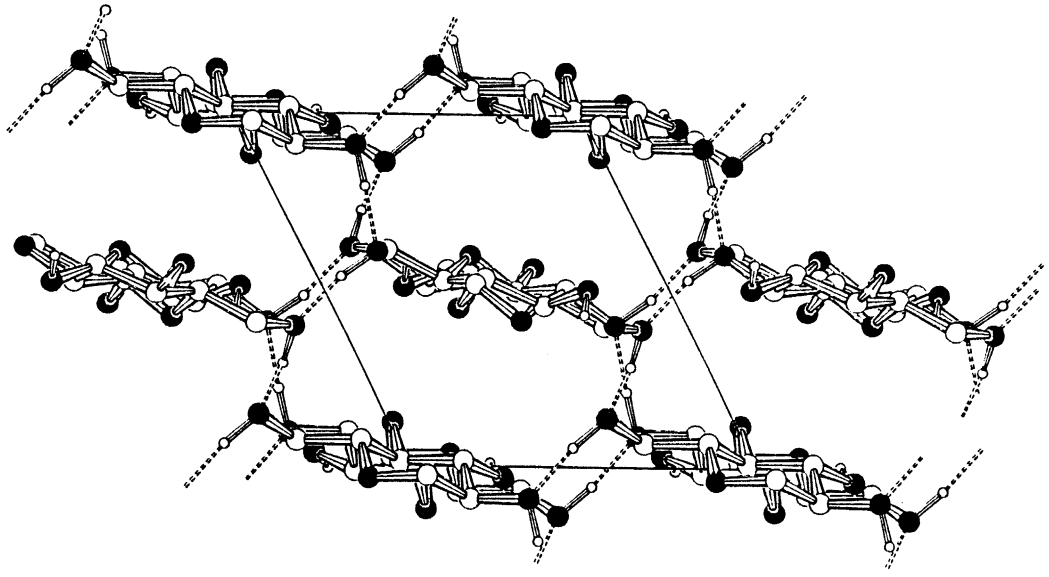

CELLULOSE II

Fig. 2. The crystal structure of cellulose I and cellulose II viewed along the chain axis. Dashed lines indicate intermolecular hydrogen bonds.

hence the value of g. This effect has been demonstrated for PpPTA and cellulose fibres [60]. This variation in g has implications for the graph of birefringence versus sonic compliance. For well-oriented fibres with a Gaussian distribution of chain orientation $\langle \sin^2\phi \rangle_E \approx \langle \sin^2\phi \rangle$, whereas for an affine orientation distribution $\langle \sin^2\phi \rangle_E \approx 3/4\langle \sin^2\phi \rangle$. An affine distribution is found in medium and low oriented cellulose fibres [46]. Say that $\langle \sin^2\phi \rangle_E = r\langle \sin^2\phi \rangle$ and

$$f = 1 - \frac{2g(1 + \nu_{13})}{e_c} \tag{5}$$

it follows that the relation between the birefringence and the

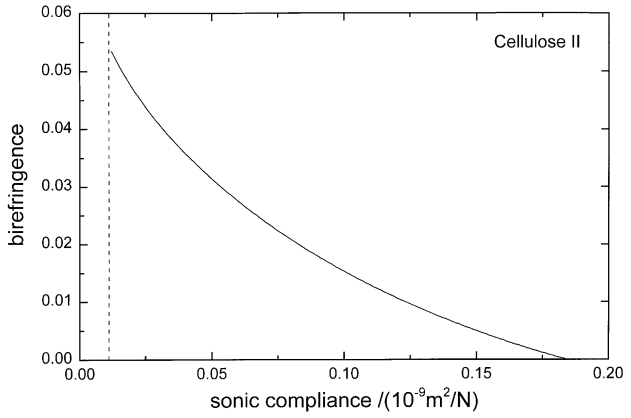

Fig. 3. The birefringence versus the sonic compliance according to Eq. (6). The dashed line is drawn at $E^{-1} = e_c^{-1}$.

modulus can be derived from Eqs. (1) and (2)

$$\frac{\Delta n}{\Delta n_{\max}} = 1 + \frac{3g}{rfe_c} - \frac{3g}{rfE}. \tag{6}$$

Eq. (6) shows that in principle the ratio of the slope to the intercept is, approximately, $-3g$. However, as discussed above, g is likely to be a function of the orientation for the whole range of cellulose fibres, i.e. from unoriented to highly oriented. Hence, a plot of Δn versus E^{-1} will yield a curve with a decreasing slope [57,60]. A numerical evaluation of Eq. (6) is accomplished as follows. The gradual change from a Gaussian distribution for highly oriented fibres to an affine distribution for low oriented fibres is expressed by the empirical relation $r = -1.32/E + 1$. The functional dependence of g on the degree of orientation is described by the empirical relation $g = 1.3 \ln(E) - 0.8$, which is supported by the experimental results given in this study. Taking a Poisson's ratio $\nu_{13} = 0.3$ and $\Delta n_{\max} = 0.0545$ for conditioned fibres the relation between Δn and E^{-1} depicted in Fig. 3 is obtained.

Besides the chain orientation relative to the fibre axis, also called the axial texture, wet spun fibres often show a lateral texture [16,46]. If they do specific lattice planes parallel to the chain axis show a preferred orientation in the cross-section of the filament. Three principal modes are distinguished, viz. radial, tangential and random orientation. Skin–core differentiation in the fibre should also be considered as a possible parameter influencing fibre properties, such as torsional modulus and transverse strength. Lateral texture and skin–core differentation may affect the fibrillation properties of the fibre.

Lateral texture in the filament cross-section can be detected by light miscroscopy or electron diffraction. The directional dependence of the polarizability of the cellulose chain in the plane formed by the a and b axes is supposed to have its largest value approximately along the longest dimension of the chain cross-section, and its smallest value perpendicular to it. It follows that n_α is directed approximately along the bisectrix of the angle between the $[1\bar{1}0]$ and [100] directions, and n_β perpendicular to this bisectrix. This paper will show that this hypothesis is in agreement with the lateral birefringence measurements on filament cross-sections in conjunction with the results obtained from electron diffraction on oblique or almost longitudinal filament sections.

Lateral texture may be the cause for a particular fracture morphology. Apart from inhomogeneities such as voids, the mechanical anisotropy of the crystal structure of cellulose II in conjunction with a specific kind of lateral texture can lead to radial fracture of the filament. Fig. 2 illustrates that each monomeric unit in the crystal structure of cellulose II is bonded by four pairs of hydrogen bonds to its neighbours, which at first sight suggests that a preferred cleavage direction in the **a**, **b** plane is unlikely. Yet, radial cleavage in the cross-section of cellulose II filaments has been observed. This suggests that, in spite of the hydrogen bonding in several directions, preferential directions for cleavage of hydrogen bonds between the chains do exist. Assuming a crack in the direction r, the associated rupture strength σ_{rs} in a direction r' perpendicular to r, is given by the equation

$$\sigma_{rs} = \sqrt{\frac{2E\gamma}{d_0}}, \tag{7}$$

where E is the modulus parallel to r', γ the surface energy of the potential cleavage planes parallel to r, and d_0 the distance between these planes [70]. Four possible cleavage directions in the a, b plane are considered, viz. [100], [110], $[1\bar{1}0]$ and [310]. It is assumed that for a possible cleavage direction r the relevant modulus along r' is proportional to $\sum \cos\vartheta$, where ϑ is the angle between direction of the hydrogen bonds considered and r', and the summation being taken per unit length along r and per length of the c axis. The surface energy γ of a possible cleavage plane is supposed to be proportional to the number of hydrogen bonds per unit length along r and per length of the c axis. Other relevant data for the calculation of σ_{rs} are the distances between the molecules d_m in the parallelogram ABCD formed by the centers of the four corner molecules shown in Fig. 4: AC/2 = 0.45 nm, DB/2 = 0.74 nm and AB = $|a|$ = 0.8 nm. The results of the calculations are presented in Table 1.

As an example, the possible cleavage direction [110] is considered using the projection of the crystal structure in Fig. 4. Along the line $\{(1/2,0,0) + (1/2a,1/2b,0)\}$ and over a distance equal to AC/2 there are four hydrogen bonds between neighbouring chains. Of these bonds two make an angle of about 70° with r' or the normal to [110], one is almost parallel to r, and one subtends an angle of about 45° with r. Hence, $E \propto (2\cos 70° + \cos 45°)/(AC/2)$ and $\gamma \propto 4/(AC/2)$, while $d_0 = d(1\bar{1}0) = 0.72$ nm, so that $\sigma_{rs} \propto 8.8$. Moreover, as the projection of the anhydroglucose unit on to the a, b plane subtends an angle of about 20° with the normal to [110], its contribution to the modulus

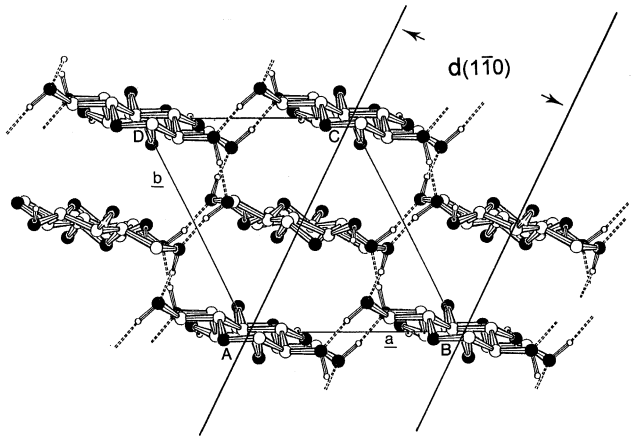

Fig. 4. The hydrogen bonding between the chains in cellulose II seen along the chain axis together with the 1$\bar{1}$0 planes.

along this direction, though in a series arrangement, will be considerably larger than for the other directions. The difference between the value of the rupture strength pertaining to the cleavage direction along [110] and the rupture strengths of the other directions is therefore likely to be larger than the values given in Table 1. From these considerations it follows that the most likely cleavage directions are parallel to the [100] direction or the a axis and parallel to the [1$\bar{1}$0] direction. The proposed directions of n_α and n_β, and the cleavage directions relative to the a and b axes are shown in Fig. 5.

So far we have discussed the morphological features of the cellulose fibres, which are related to the mechanical properties according to a well defined model based on the series approximation, the chain orientation and the mechanical anisotropy of the crystal structure. However, there are some structural features for which the relation with the mechanical properties is less well established. Almost all wetspun fibres show an equatorial small-angle X-ray scattering indicating the presence of elongated voids parallel to the fibre axis with transverse dimensions less than about 200 nm. Larger elongated voids in these fibres are sometimes observed with confocal laser microscopy and transmission electron microscopy. Presumably, these voids, together with the lateral texture discussed above, affect the fibrillation behaviour, the torsional modulus, the transverse strength and to some extent also the tensile strength of the fibre.

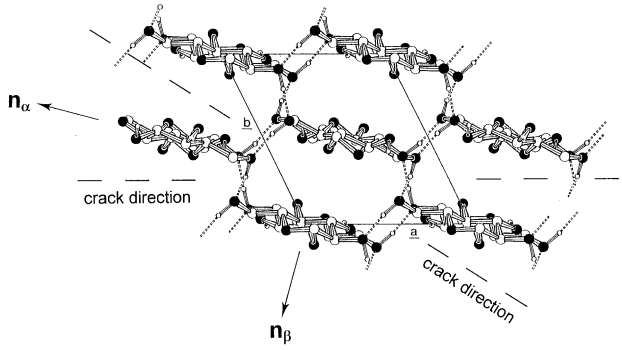

Fig. 5. Proposed directions for n_α and n_β and for the crack planes parallel the chain axis.

3. Experimental

3.1. Preparation of the spinning solution

The strength of orthophosphoric acid as a solution of phosphorus pentoxide (P_2O_5) in water, can be expressed in a P_2O_5-concentration (72.4% w/w). Beyond this point waterfree conditons are reached. Such conditions can for instance be obtained by mixing two or more of the following components: orthophosphoric acid, pyrophosphoric acid, polyphosphoric acid, phosphorus pentoxide, and water. Though anisotropy was established over a wider range, the optimum results were obtained for a P_2O_5 concentration in the solvent between 72 and 76% w/w. The solutions were already anisotropic above a cellulose concentration of 8% w/w, which is extremely low for this polymer taking into account the semiflexible nature of its chain. This critical concentration is comparable to the one for a polymer as rigid as PpPTA dissolved in sulfuric acid [18]. This cellulose solution therefore seems highly suitable for the production of high modulus, high tenacity yarns.

3.2. Raw materials

Orthophosphoric acid: Font electrique SA Bex 99% H_3PO_4.

Polyphosphoric acid: Albrite approx. 84% P_2O_5

Cellulose: powdered Buckeye V60

Orthophosphoric and polyphosphoric acid were mixed in such a ratio in a thermostated vessel that the solvent had a concentration of approximately 74% w/w P_2O_5. During mixing the temperature was held above 42°C in order to

Table 1
Estimation of the rupture strength values for possible cleavage planes

Cleavage along	d_0 (nm)	E (a.u.)	γ (a.u.)	$\sigma_{rs} = \sqrt{(2E\gamma/d_0)}$ (a.u.)
[110]	d (1$\bar{1}$0) = 0.72	3.1	8.9	8.8
[1$\bar{1}$0]	d (110) = 0.44	2.7	2.7	5.8
[100]	d (020) = 0.40	2.45	2.5	5.5
[310]	d (130) = 0.22	1.8	2.7	6.6

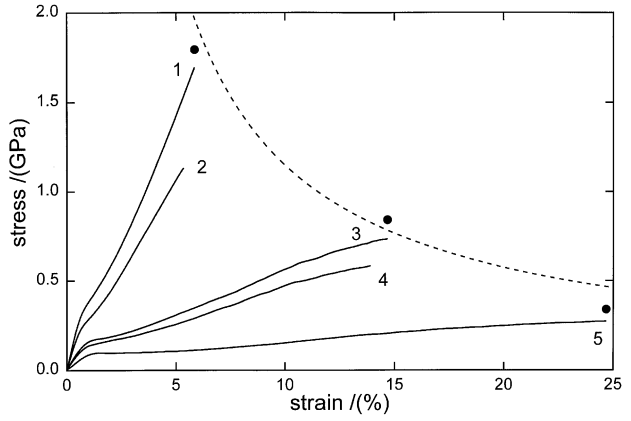

Fig. 6. The tensile curve for a test length of 100 mm of the strongest filament in a yarn of: (1) Fibre B and the viscose fibres, (2) Cordenka EHM, (3) Cordenka 700, (4) Cordenka 660 and (5) Enka Viscose. The solid dots indicate the stress related to the reduced cross-section at fracture. The hyperbola-shaped failure envelope represented by the dashed line has been fitted to the data points shown as solid dots.

melt the phosphoric acid crystals and equilibrate the mixture. Powdered cellulose with an equilibrium moisture content of approximately 5% w/w and the solvent were thoroughly mixed in a ZSK 30 twin-screw extruder. The solution, containing 19% w/w of dry polymer, was filtered, heated and extruded through an assembly of spinnerets, containing 1500 capillaries of 65 μm. The filaments passed through an air gap, in which they were subjected to stretching, and went through a falling jet coagulation bath of acetone of 5°C. The acid was further removed from the yarn by washing with water in jet washers to achieve a phosphorus level of 0.43% w/w P, part of which appeared to be bonded to the cellulose. Turbak's objection to this process, that it would be extremely hard to isolate the cellulose from a phosphoric acid solution, has thus been overcome [38]. The yarns were neutralized with a 2% w/w Na_2CO_3 solution, washed untill a sodium content of 0.53% w/w Na and finished and dried on heated godets at a speed of 100 m/min. The degree of polymerization (DP), as determined by a viscosity measurement in copper II ethylene diamine/water mixture, was 620, whereas the raw material had a DP of approximately 800, indicating that degradation, despite the use of a strong acid as a solvent, is not an important factor [6]. Because of the high rate of dissolution, in contrast with the slow rate found in the preparation of viscose, short process times can be realized, which is advantageous for economic processing.

The structure and mechanical properties of the new fibres coded B are compared with the following cellulose fibres: a textile yarn Enka Viscose, Cordenka® 660 and 700 tyre yarns, a high modulus Cordenka® EHM yarn, which are all made according to the viscose process, and with an old sample of Fortisan® yarn made by spinning a cellulose acetate yarn, which was stretched up to 2000% in saturated steam and subsequently saponified in sodium acetate, washed, and dried [5,71]. For the determination of the lateral texture by electron diffraction a fibre sample coded A, was used that was obtained by spinning a cellulose fibre from an anisotropic solution of a mixture of phosphoric acid and formic acid [72].

Table 2
The sonic modulus and the average filament tensile properties measured at a test length of 10 cm and a strain rate of 10%/min, with estimated standard deviations in parentheses referring to the last digit. The test length for the Fortisan sample was 2.5 cm

Fibre	E_{son} (GPa)	E_{in} (GPa)	σ_b (GPa)	ϵ_b (%)
Viscose textile	15	9.3 (2)	0.26 (2)	23.5(2)
Cordenka® 660	22	17.3 (4)	0.51 (6)	12 (2)
Cordenka®700	24	18.9 (5)	0.6 (1)	12 (2)
Cordenka®EHM	49	38 (1)	0.9(2)	4.6(7)
Fortisan®	45	32 (2)	1.0(1)	6.8(5)
B	58	45 (5)	1.3 (3)	5.1 (9)

3.3. Mechanical properties

Tensile measurements have been performed with the Zwick 1445 Tensile Tester at 21°C and 65% R.H. Test lengths of 25 and 100 mm with a strain rate of 10%/min. have been applied. The count of the individual filaments was determined with a vibroscope. Fig. 6 shows the tensile curves of the strongest filaments in a yarn for the test length of 100 mm of the fibres made with the viscose process and fibre B. The observed values averaged for the 10 strongest filaments among 50 filaments of fibre B at a test length of 25 mm, with sample standard deviations added in parentheses, are: strength $\sigma_b = 1.70(0.03)$ GPa, initial modulus $E_i = 44(3)$ GPa, elongation at break $\epsilon_b = 6.5(0.3)\%$ and the count is 1.43 (0.16) dtex. Table 2 lists the average filament tensile properties of the fibres. Sonic modulus versus strain measurements at 21°C and 65% R.H. were obtained using a yarn length of 2 m. Fig. 7 shows the curves for Cordenka® 700 and fibre B measured during loading and unloading.

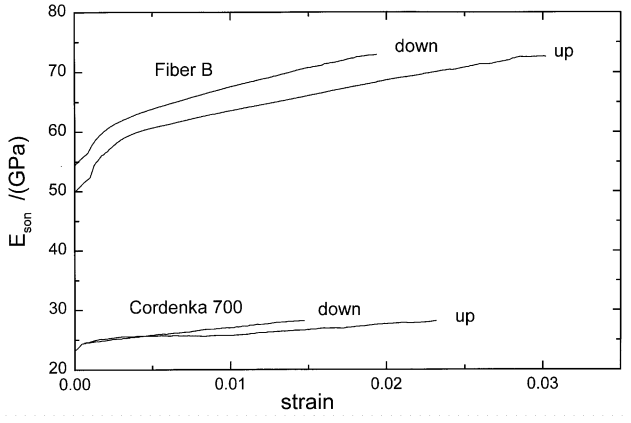

Fig. 7. The sonic modulus for increasing and decreasing strain for fibre B and the Cordenka® 700 fibre measured at 21°C and 65% R.H.

Table 3
Crystal sizes derived from the $1\bar{1}0$ and the 004 reflections, and g values of the various cellulose II fibres

Fibre	Crystal width (nm)	Crystal height (nm)	g (GPa)
Viscose textile	2.9	9.0	1.8
Cordenka® 660	3.6	10.3	2.6
Cordenka® 700	3.7	9.6	2.4
Cordenka® EHM	4.3	15	2.8
Fortisan®	5.5	15.6	
B	3.9	17.8	3.8

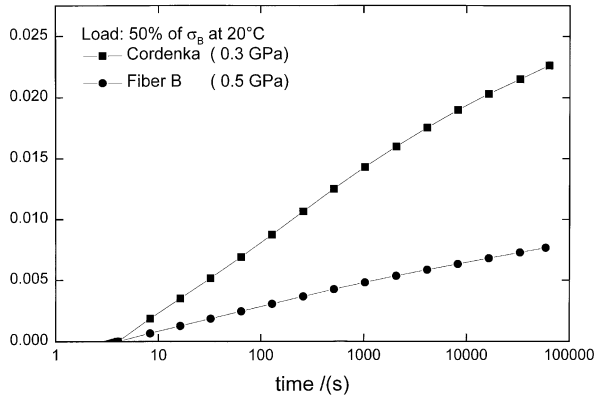

Fig. 8. The creep of fibre B compared with the Cordenka 700 fibre, both have been measured on yarns at 21°C and 65% R.H.

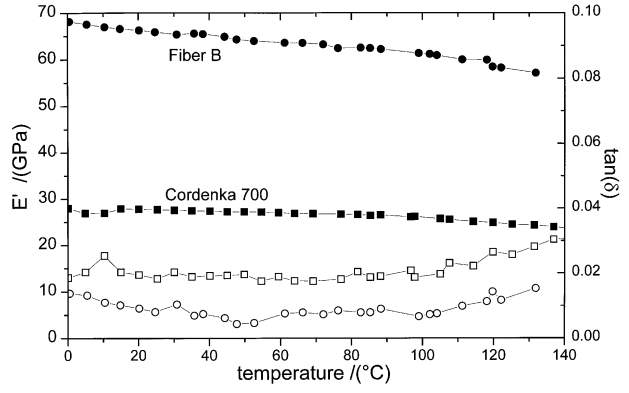

Fig. 9. Dynamic mechanical analysis as function of the temperature of fibre B and Cordenka® 700, both fibres being thoroughly dried before the measurement, prestress 170 MPa, frequency 100 Hz, strain amplitude 0.05% and nitrogen atmosphere. Solid dots are the moduli and open dots are the tan δ values.

Table 3 lists the values of the shear modulus g derived from these curves. Fig. 8 presents the creep curve of fibre B and Cordenka® 700 at 21°C and 65% R.H. A graph representing the dynamic modulus of a bone dry fibre in nitrogen environment as a function of the temperature is shown in Fig. 9. The hysteresis loss of the cellulose B fibre is compared with Cordenka 700, PpPTA, polyamide 6 and PET fibres in Fig. 10.

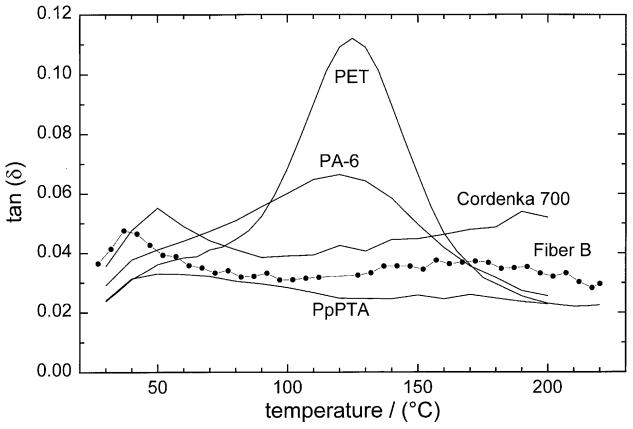

Fig. 10. The hysteresis losses as a function of the temperature for the cellulose B fibre compared to PpPTA, polyamide 6 and PET fibres.

Table 4
Axial birefringence and lateral birefringence of the cellulose fibres

Fibre	$10^4\,\Delta n$	$10^4\,\Delta n_{lat}$
Viscose textile	260	18[a]
Cordenka®660	330	22
Cordenka®700	390	18
Cordenka®EHM	510	13
Fortisan®	480	0
A	495	44–67
B	502	16

[a] Sections of the viscose filaments are noncircular and the lateral birefringence does not indicate radial texture but refers to preferred orientation in domains.

3.4. Optical investigation

For the optical investigation a Jenapol Interphako-U polarization microscope was employed. In the case of filaments with a perfect circular cross-section the axial birefringence $\Delta n = n_{\parallel} - n_{\perp}$ was determined with the De Senarmont method using dibutylphthalate as an immersion liquid [73]. In the case of noncircular cross-sections, the refractive index, in both the parallel and perpendicular direction, was determined with an interference microscope by compensation with Cargille solutions using interference microscopy. The results are presented in Table 4. As wet-spun fibres often show lateral texture as a result of coagulation the lateral birefringence of fibre B and other cellulose II fibres was determined. To obtain cross-sections the fibre bundle was embedded in Spurr low viscosity embedding material and allowed to harden for at least 16 h at 70°C. Sections normal to the fibre axis of about 2 mm thickness were prepared using a Struers Accutom. The sections were ground and polished down to a thickness between 10 and 40 μm, and cemented to a microscope glass slide with Locktide IS 401. The thickness of the section was determined using a 100× planachromatic immersion objective. The retardation was measured with De Senarmont's method

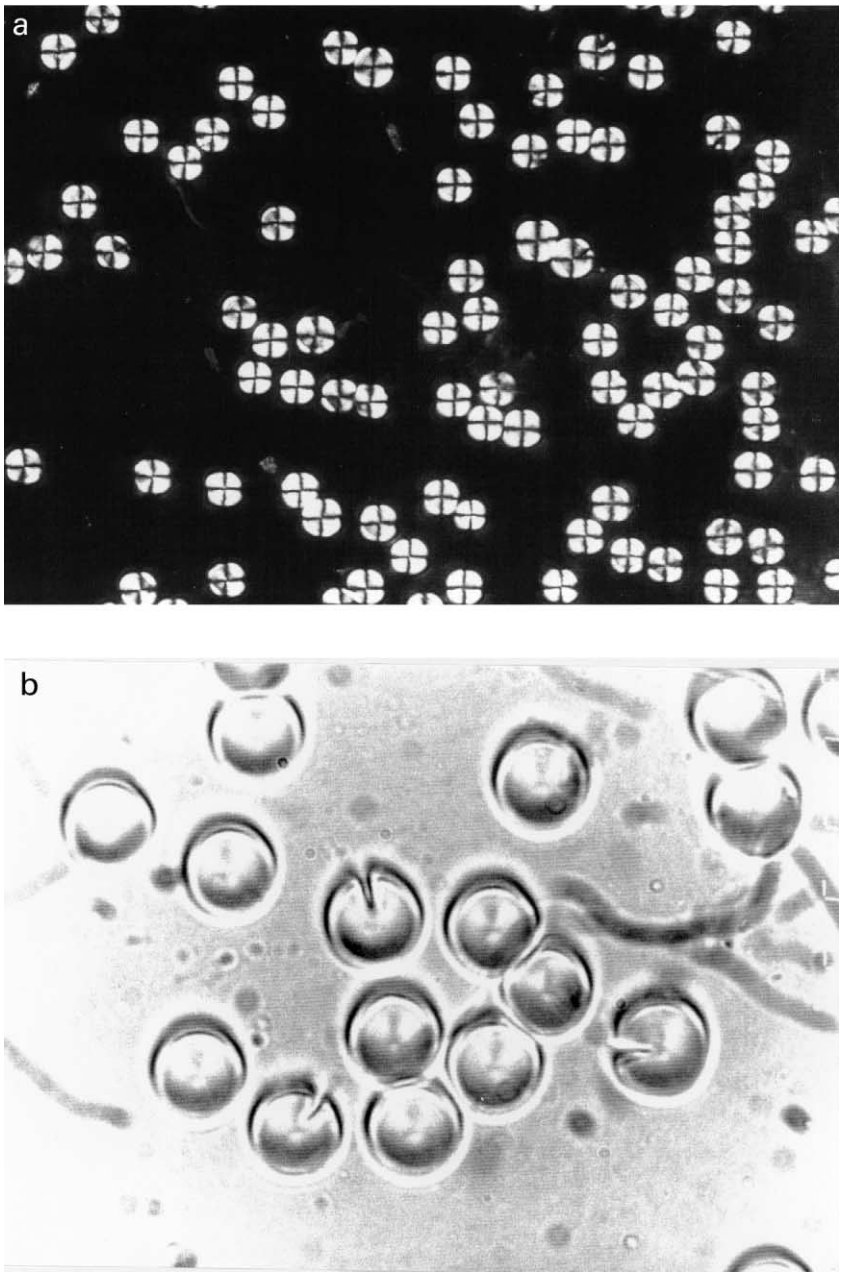

Fig. 11. (a) Optical micrograph of sections of fibre A between crossed polars showing positive lateral birefringence, (b) optical micrograph showing the radial cracking.

of compensation using monochromatic light from a Xenon light-source with a DISP-546 monochromator. Fig. 11 shows optical micrographs of a section of fibre A. Positive birefringence was detected by employing a lambda compensating plate. The results for fibre B, Fortisan, and a number of viscose yarns are presented in Table 4. Due to the anisotropy of its crystal structure, cellulose II has three refractive indices: n_γ parallel to the c axis, and n_α and n_β perpendicular to this axis. The lateral birefringence, $\Delta n_{\text{lat}} = n_\alpha - n_\beta$, is a measure of the structural anisotropy or lateral texture in the filament cross-section. In the case of cellulose, the difference between n_α and n_β is expected to be small, and the orientation of the optical axes α and β relative to the a and b axes is not known. Yet, in order to establish the kind of lateral texture in the filament it is necessary to know this orientation. Therefore, it was decided to use electron diffraction for the determination of the lateral structure of fibre A, which has a relatively large value for lateral birefringence and hence a pronounced lateral texture.

3.5. Wide-angle X-ray diffraction

The X-ray diffraction pattern taken with a flat plate

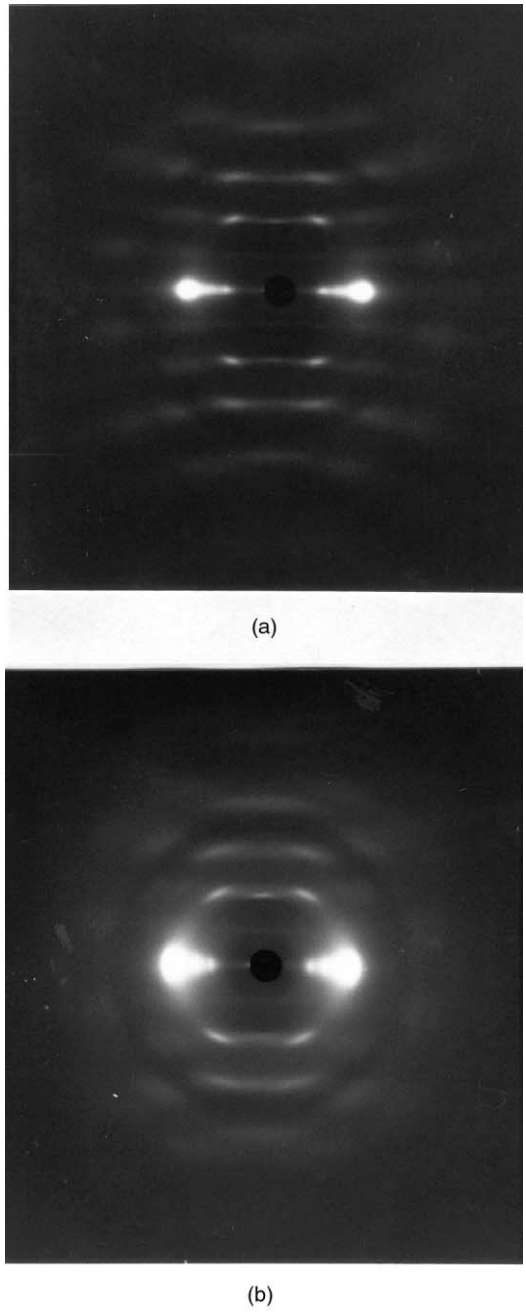

Fig. 12. The X-ray diffraction patterns taken with a flat plate camera of: (a) fibre B, and (b) the Cordenka® 700 tyre yarn.

camera and Cu Kα radiation of fibre B spun from an anisotropic solution in phosphoric acid is shown in Fig. 12a. Fig. 12b shows the pattern taken with the same camera and radiation of a commercially available Cordenka® 700 cellulose tyre yarn. The differences in orientation and crystallinity are striking. Both patterns are characteristic of the cellulose II crystal modification. Table 3 presents some structural parameters of the various cellulose fibres. Slight derivatization by cellulose phosphate is manifested by a diffuse intensity between the $1\bar{1}0$ and the 110 reflection and by a smaller crystallite width derived from the $1\bar{1}0$

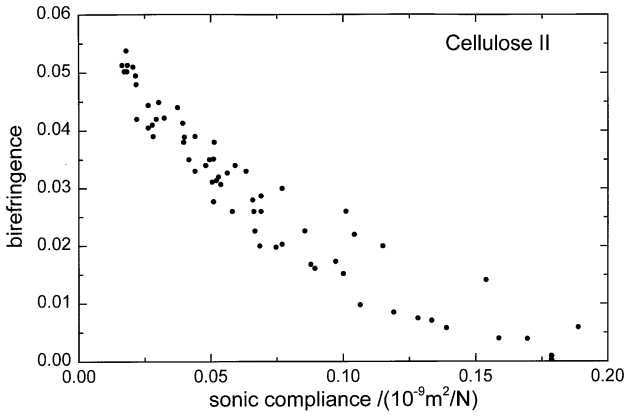

Fig. 13. The birefringence versus the sonic compliance including the data by de Vries and the fibres investigated in this study.

reflection than observed for other cellulose fibres with a similar degree of orientation.

3.6. Small-angle X-ray diffraction

The small-angle diffraction pattern with a resolution up to 80 nm did not show a meridional reflection, indicating that a periodic morphology of crystalline and amorphous domains along the fibre direction is unlikely. From equatorial small-angle X-ray scattering and confocal laser scanning microscopy it was found that fibre B had very few pores compared to the viscose fibres.

3.7. Electron diffraction

Filaments were clamped in the incisions of a BEEM flat mould capsule (ex Agar). For oblique or longitudinal sections these incisions were made perpendicular to the longer axis of the capsule, which was aligned along the filaments. The ratio of long axis to the short axis of the elliptic shaped sections was greater than 10. The filaments were embedded in a water-soluble Nanoplast FB 101 (ex Agar) melamine resin, using the medium hardness version by mixing 10 g of MME 7002 with 0.20 g B52. The resin was cured for two days at 40°C in a container with silicagel in a nitrogen atmosphere. After curing, the amount of resin was decreased and the moulds were refilled. Another curing treatment was performed at 60°C for two days. The blocks with the filaments were removed from the mould and positioned in a Reichert Ultracut S ultra-microtome using a diamond knife with a 45° edge. Sections of 100 nm were collected on a 200 mesh Cu grid and coated in high vacuum with a thin layer of carbon on both sides. Selected area electron diffraction (SAD) patterns were obtained at 120 kV with a Philips 400 T transmission electronmicroscope (TEM) combined with a Gatan camera and a low dose unit. The very low intensity of the illumination was adjusted to a spot of about 5 μm. The conventional SAD patterns were taken from an area of 2 μm from the centre of the illumination. The noisy diffraction patterns were integrated during 20 s

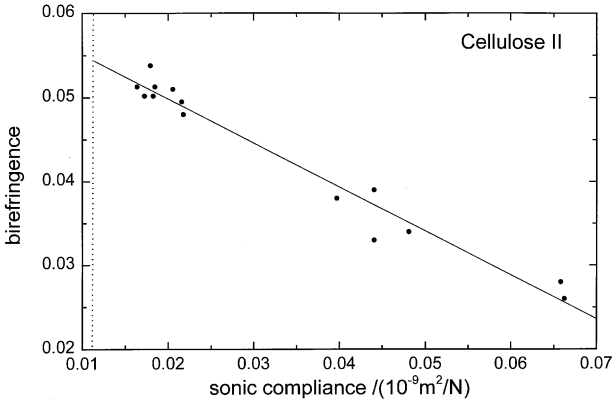

Fig. 14. The birefringence versus the sonic compliance for fibres with $E^{-1} < 0.07$. The dashed line is drawn at $E^{-1} = e_c^{-1}$.

with the aid of a Quantel Crystel image processing system. For every observation a new area of a section was used. As cellulose structures are very sensitive to electron beam radiation the procedures were checked by taking more diffraction patterns from the same spot. In general, the reflections in the pattern started to fade away by beam damage after about 1 min. Diffraction patterns were also made with a Jeol 2010 transmission electron microscope operated at 200 kV with a Gatan CCD camera and a minimum dose system, using a beam spot size of about 5 μm. With this system similar information from the patterns was obtained as with the Philips TEM.

4. Results and discussion

The modulus and tenacity of the cellulose fibre B are considerably higher than those obtained by the saponified acetate process. Sprague and Noether reported the following maximum filament values for these fibres: an initial modulus of 41 GPa, a tenacity of 1.08 GPa, and an elongation at break of 5.6% measured with a gauge length of 6 cm at 23°C and 65% RH [5]. The Fortisan® saponified acetate fibre is highly oriented and highly crystalline as shown by the well-defined spots on the X-ray diffraction pattern. In comparison the highly oriented fibre B is slightly less crystalline due to the presence of a minor amount of phosphorus. Fig. 13 shows a plot of the birefringence and sonic compliance data of this investigation together with all the data measured by de Vries on viscose and model filaments [74–76]. Good agreement is found between the experimental data and the theoretical curve shown in Fig. 3, which has been calculated using relations between r, E, and g that closely approximate the experimental relations found in this study. For isotropic cellulose fibres de Vries found a sonic modulus of 5 GPa by extrapolation to $\Delta n = 0$. For isotropic fibres, $\langle \sin^2 \phi \rangle_E = 0.5$ and Eq. (1) yields $E_{iso} \cong 4\,g$, which means that $g_{iso} = 1.25$ GPa. Fig. 14 presents a plot of Δn versus E^{-1} for the medium and highly oriented fibres (1/E < 0.07), of which some are listed in Tables 2 and 4. De Vries's data have not been included in this graph. Linear regression yields $\Delta n_{max} = 0.0545$, and the ratio of the slope to the intercept is −8.7, yielding a value of 2.9 GPa for g. All values refer to conditions of 65% RH and 21°C. It has been reported that the shear modulus of well-oriented cellulose I fibres, $g = 1.5$ GPa, was found smaller than that of the cellulose II fibres for which $g = 2.5$ GPa [57]. The value for the shear modulus of the well-oriented cellulose II fibres, $2.4 \leq g \leq 3.8$ GPa, obtained in this investigation with the method based on Eq. (3) confirms this result. The g of cellulose II is also considerably higher than for the poly(p-phenylene terephthalamide) or PpPTA fibres, for which $1.4 \leq g \leq 2.8$ GPa. This is presumably due to the bidirectional hydrogen bonding network in the cellulose II crystal compared to the unidirectional hydrogen bonding in the cellulose I and PpPTA crystal structures [60,65]. Thus the average shear modulus of the cellulose II fibre should be larger than the average shear modulus in cellulose I and PpPTA fibres, for which it is an average of the large value g_H in the hydrogen bonded plane and the g_W for the van der Waals interactions between the hydrogen bonded planes. Kroon-Batenburg calculated a value of 4 GPa for the g_H of PpPTA, which is very close to the g value of fibre B [16]. Interchain bonding is not only determined by the kind of hydrogen bond network but also by the crystal perfection as is demonstrated by the correlation between g and the crystal height given in Table 3. The crystal height is calculated from the width of the meridional reflections and can be interpreted as a measure of the distance along the chain of more or less perfect order of the interchain hydrogen bonding. It should be noted that there is no correlation between g and crystal width. However, g is affected by the water content in the fibre. As shown by Fig. 9, the dynamic modulus of a dry fibre B at 21°C is 67 GPa. Assuming that the chain orientation is not changed by the drying process Eq. (6) yields a value of 6.2 GPa for g. This value is not much different from the value of 7.2 GPa found for the new rigid-rod polymer fibre poly{2,6-diimidazo[4,5-b:4′5′-e]pyridinylene-1,4(2,5-dihydroxy)phenylene), which also has a bidirectional hydrogen-bonded network [17,77–79]. This analysis of the relations between the structure, the orientation parameter, the shear modulus g, and the fibre tensile modulus demonstrates that the mechanical properties of the cellulose fibres are well described by the continuous chain model.

When polymer fibres are extended beyond the yield strain, plastic deformation occurs. For PET and PpPTA fibres an increase in initial modulus is observed after unloading, which is caused by plastic rotation of the chains. As shown in Fig. 7, unloading after extension of cellulose II fibres does not result in a significant increase in the initial modulus, although a finite plastic deformation clearly occurs. For example, in the case of Fibre B a permanent strain of 1% is observed after extension up to 3%. This cannot be due to plastic rotation of chains, as the initial

Table 5
Potential reflections to be observed on the ED pattern of a cellulose II fibre. The observed structure factors F_{hkl} are according to Kolpak and Blackwell [80]

Miller index	Lattice spacing (nm)	Observed F_{hkl} (a.u.)
$1\bar{1}0$	0.721	45
110	0.443	95
020	0.402	100
030	0.268	11
$\bar{1}40$	0.222	26
002	0.518	Moderate
012	0.436	29
013	0.317	24
004	0.255	Strong

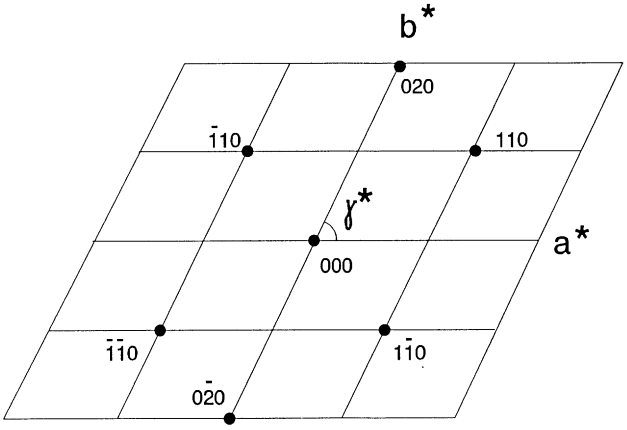

Fig. 15. The reciprocal lattice indicating the observable *hk*0 reflections.

modulus, obtained by extrapolation to zero strain, remains almost constant. Considering the strong bidirectional lateral bonding between the chains in cellulose II, we believe that the permanent strain is caused by chain slip. In contrast with cellulose II, planes containing strong secondary bonds between the chains separated by van der Waals interactions are found in PET and, in particular, hydrogen-bonded planes are found in PpPTA. Due to the weaker van der Waals bonds between these planes, plastic rotation resulting in an increase in initial modulus is likely to be confined to shear of these planes.

Figs. 8–10 show the viscoelastic properties of fibre B compared with PET, PA-6, PpPTA and another cellulose fibre. Similar to the PpPTA fibres, fibre B has a logarithmic creep, a low value for tan δ, and like other cellulose fibres also a modulus that only slightly depends on the temperature.

Fig. 6 shows that the endpoints of the tensile curves of the different cellulose fibres lie approximately on a hyberbolic shaped failure envelope. This shape can be explained by assuming that the area under the tensile curve is constant for these fibres. The work supplied to the fibre per unit volume of the undeformed fibre is given by

$$W = \int_0^{\epsilon_b} \sigma \, d\epsilon. \tag{8}$$

Suppose that the tensile curve is approximated by the linear relation

$$\sigma = E' \epsilon, \tag{9}$$

where E' is the apparent modulus, then the equation for the failure envelope becomes a hyperbola

$$\sigma_b = \frac{2W}{\epsilon_b}. \tag{10}$$

The degree of polymerization of the cellulose of fibre B and Cordenka 700 is about 600 and considerably larger than the DP of the Enka Viscose fibre, which is about 400. Hence, in the fitting of Eq. (10) the fracture points of fibre B and Cordenka 700 were given more weight yielding the dashed curve in Fig. 6 with $W = 0.058$ GJ/m^3. Except for the highly oriented fibres, the work to fracture consists mainly of strain energy of the interchain bonds. The energy of a hydrogen bond is about 30 kJ/mol and there are 8 intermolecular hydrogen bonds in the unit cell of 668×10^{-30} m^3 yielding a total energy of 0.596 GJ/m^3. Apparently the work neccessary to break a well-made cellulose filament with a DP of 600 is about 10% of the total energy content of the intermolecular hydrogen bonds.

For the determination of the directions of the optical axes n_α and n_β relative to the crystal structure, very thin longitudinal sections were prepared. In case of electron diffraction (ED) on longitudinal and transverse sections of filaments with an axial orientation of the *c* axis, only the crystal planes that are approximately perpendicular to the surface of the section will diffract the primary beam of electrons. For random orientation of the *hk*0 planes in the cross-section of the filament the intensity ratio of the *hk*0 reflections will closely approximate the intensity ratio of the X-ray diffraction pattern of the fibre. The intensities of the strongest reflections of cellulose II according to Kolpak and

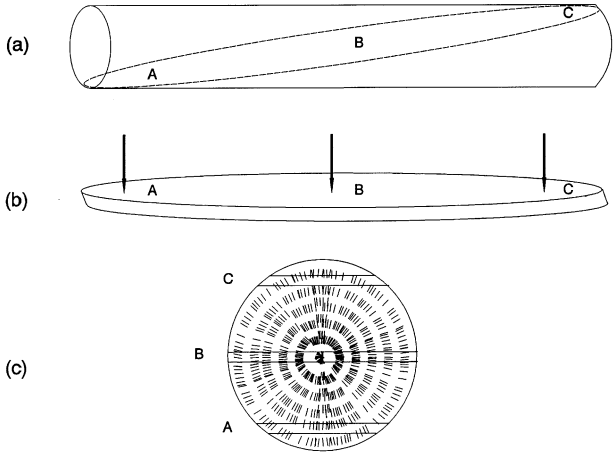

Fig. 16. Schematic presentation of an oblique section with a small angle to the axis of a filament with radial texture of a specific lattice plane, showing the beam direction and the variation of orientation of these planes relative to the section surface for different locations.

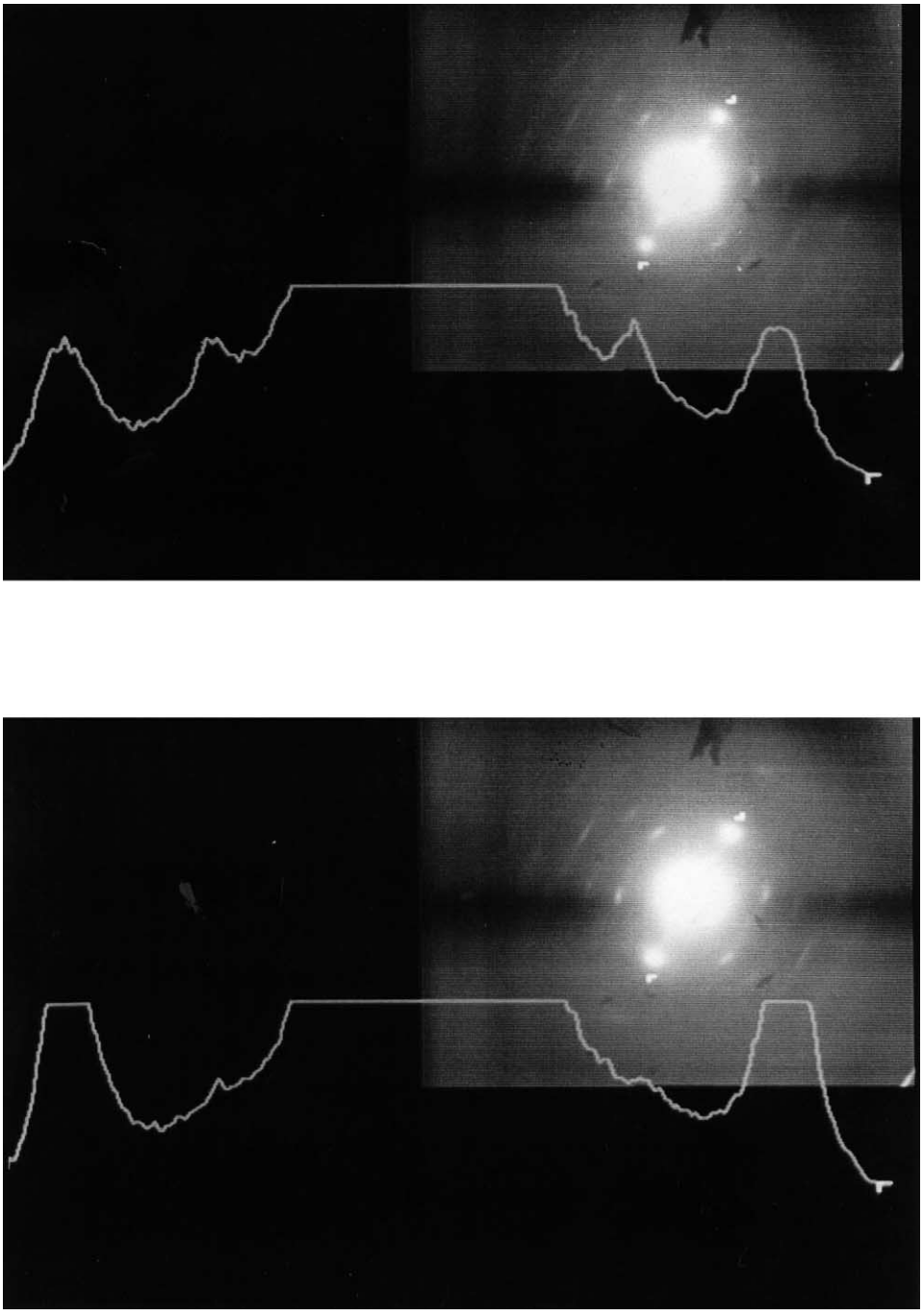

Fig. 17. The ED patterns and the equatorial intensity profile taken between the two white markers from an oblique section through a filament of Fibre A with radial texture of the 110 planes in the cross section. Top: the pattern for the center position of the section showing the presence of $1\bar{1}0$ reflection and the relatively low peak of the unresolved 110 and 020 reflections. Below: the pattern for the position near the focal point of the elliptic shaped section showing the absence of the $1\bar{1}0$ reflection and the strong peak of the unresolved 110 and 020 reflections.

Blackwell are listed in Table 5 [80]. The intensities and d-spacings of different cellulose yarns may show gradual differences; for example a low degree of lateral crystalline order may result in a fusion of the main two equator reflections 110 and 020.

The positions and the occurrence of reflections due to lateral texture in the ED patterns is perhaps best explained by making use of the concept of the reciprocal or diffraction space. In this space the reflections are positioned on the nodal points of a lattice defined by the reciprocal axes a^*, b^* and c^*. The vectors to the nodal points hkl in this reciprocal lattice are parallel to the normals onto the lattice planes in the crystal. Fig. 15 depicts the reciprocal lattice with the observable $hk0$ reflections indicated by black dots. Actually, these reflections are arc-shaped due to the finite crystallites and the azimuthal distribution in polymer fibres. The extent

Table 6
Comparison of the average filament strength and moduli, normalized for the chain modulus, for cellulose II fibres spun from an anisotropic solution in phosphoric acid, PpPTA and PBO fibres supplied by Toyobo

Fibre	e_c (GPa)	E_f (GPa)	E_f/e_c	σ_b (GPa)	σ_b/e_c
Cellulose II (B)	90	44	0.49	1.3	0.0144
PpPTA (Twaron®1055)	240	120	0.50	3.2	0.0133
PBO	475	280	0.59	5.8	0.0122

of the arc reflects the degree of lateral texture in the filament cross-section. In case of complete random texture around the *c* axis these arcs become full circles around the origin of the reciprocal lattice.

Fig. 16 depicts the oblique section through a filament with a small angle to the filament axis. For radial orientation in the filament cross section of a specific lattice plane parallel to the filament axis the orientation of this plane relative to the surface of the elliptic section depends on the position in the section. Consequently, depending on the location of the primary beam spot, the ED pattern will show variation of the intensities of certain planes. For example, for radial orientation of the 110 planes in the filament the ED pattern taken with the beam normal to the section in the centre position B will show a fibre pattern with a maximum intensity of the $1\bar{1}0$ reflection and minimum or even zero intensity of the 110 and 020 reflections. This intensity ratio will be reversed for positions A and C near the focal point of the elliptic section. Fig. 17 shows both ED patterns of an oblique section of the highly oriented cellulose II fibre A with a strong lateral texture as demonstrated by a lateral birefringence of $\Delta n_{lat} = 0.006$, which fibre was made by a different process [68]. The ED patterns taken at positions A and C show the strong peak of the 110 and 020 reflection and the absence of the $1\bar{1}0$ reflection, whereas the ED pattern taken at the centre B of the section clearly showed the $1\bar{1}0$ reflection, together with a relatively weak peak of the 110 and 020 reflections. Taking into account the relative magnitudes of the structure factors listed in Table 5, the relative intensities of the $1\bar{1}0$ reflection and the 110 and 020 reflections shown by these patterns demonstrate the radial texture of the 110 lattice planes in the cross-section. Sections of this fibre sample cut normal to the filament axis displayed radial cracking as shown in Fig. 11b, which is in agreement with the expected high value of the modulus along the $[1\bar{1}0]$ direction. However, due to the angle of about 37° between the 110 and 020 planes and the azimuthal spread of the reflections some radial orientation of the 020 planes cannot be excluded. The results of the lateral birefringence measurements and the ED patterns confirm the orientation of the optical axes and the crack directions relative to the crystal axes as shown in Fig. 5. It follows that all fibres listed in Table 4, except for Fortisan, show radial texture in variable degree.

Table 6 shows that the strength and modulus, normalized by the chain modulus, of PpPTA, PBO and the cellulose B fibres are almost equal. The viscoelastic properties up to about 200°C do not show any large differences either. This underlines the similarity of the structure and morphology between the cellulose B fibre and the PBO and PpPTA fibres. It demonstrates that with regard to structure and properties the cellulose B fibre can be considered a high-modulus and high-strength fibre similar to PpPTA and PBO.

Acknowledgements

The authors wish to thank Prof. H. Chanzy of the Centre de Recherches sur les Macromolécules Végétales in Grenoble, France, for valuable advice on the preparation of longitudinal sections and the electron diffraction patterns, B. Koenders and H. Lammers for carrying out the numerous spinning experiments, Dr E. Klop and R. van Puijenbroek for small- and wide-angle X-ray diffraction characterization and the drawings of the crystal structures, Mrs Gonzalez Wientjes for optical microscopy measurements, Mrs H.C. van der Meij for the electron diffraction investigation, F. Elkink for the hysteresis measurements, and Dr R. Zegers, A. Schaap, J. Kampschreur and B. Schaffers-Korff for the mechanical measurements.

References

[1] Vollbracht L. Chemiefasern/Textilindustrie 1989;39:935.
[2] Ott E. Cellulose and cellulose derivatives, Vol. 5. New York: Wiley, 1971.
[3] Chanzy H, Paillet M, Hagege R. Polymer 1990;31:400.
[4] Sisson WA. Text Res J 1960;30:153.
[5] Sprague BS, Noether HD. Text Res J 1961;31:858.
[6] Boerstoel H, Koenders B, Westerink JB. WO 9606208 (Akzo Nobel).
[7] Kirk-Othmer. 4th ed. Encyclopedia of chemical technology, vol. 10. 1993. p. 697 New York.
[8] DE 389336 (Bemberg).
[9] Carrol-Porczynski CZ. Natural polymer man-made fibres. London: Natural Trade Press, 1961.
[10] US 3447956 (Eastman Kodak).
[11] Brandner A, Zengel HA. EP 47929 (Akzo Nobel).
[12] Buijtenhuijs FA, Abbas M, Witteveen AJ. Das Papier 1986;40:615.
[13] O'Brien JP. US 4464323 (E.I.Du Pont de Nemours).
[14] O'Brien JP. US 4501886 (E.I.Du Pont de Nemours).
[15] Villaine P, Janin C. WO 85/05115 (Michelin).
[16] Northolt MG, Sikkema D. Adv Polym Sci 1990;98:115.
[17] Sikkema DJ, Lishinsky VL. WO 9425506 (Akzo Nobel).
[18] Picken SJ, van der Zwaag S, Northolt MG. Polymer 1992;33:2998.
[19] Gray DG. Faraday Discuss Chem Soc 1985;79:257.
[20] Gilbert RD. ACS Symp Ser 1990;433:259.
[21] Gilbert RD. Handbook of fibre science and technology, International fibre science technology series 12, vol. 3. 1993. p. 357.
[22] Werbowyj R, Gray DG. Mol Cryst Liq Cryst 1976;34:97.
[23] Panar M, Willcox O. DE 2705382 (E.I. Du Pont de Nemours).
[24] Kamide K, Okajima K, Toshihiko M. DE 3035084 (Asahi).
[25] Kamide K, Okajima K, Matsui T, Kajita S. Polym J 1986;18:271.
[26] Chanzy H, Peguy A. J Polym Sci Pol Phys Ed 1980;18:1137.
[27] Navard P, Haudin JM. Br Polym J 1980;12:174.
[28] Patel DL, Gilbert RD. J Polym Sci Polym Phys Ed 1981;19:1231.

[29] Conio G, Corazzo P, Bianchi E, Tealdi A, Ciferri A. J Polym Sci Polym Lett Ed 1984;22:273.
[30] Terbojevich M, Cosani A, Conio G, Ciferri A, Bianchi E. Macromolecules 1985;18:640.
[31] Bianchi E, Ciferri A, Conio G, Cosani A, Terbojevich M. Macromolecules 1985;18:646.
[32] Bianchi E, Ciferri A, Conio G, Tealdi A. J Polym Sci Polym Phys Ed 1989;27:1477.
[33] Chen YS, Cuculo JA. J Polym Sci Polym Chem Ed 1986;24:2075.
[34] Liu CK, Cuculo JA, Allen TC, De Groot AW. J Polym Sci Polym Phys Ed 1991;29:81.
[35] Miyamoto I, Okajima K, JP 4258648 (Asahi Chemical Co.).
[36] Kamide K, Miyamoto I, Okajima K. Polym J 1993;25:453.
[37] GB 263810 (Celanese).
[38] Turbak AF, Hammer RB, Davies RE, Hergert HL. Chemtech 1980;January.
[39] Grinshpan DD, Tsygankova NG, Kaputskii FN. SU 1348396.
[40] Gmelins handbuch der anorganische chemie. 8th ed Weinheim: VCG, vol. 16C, 1965.
[41] Ullman's encyclopedia of industrial chemistry. Weinheim: VCH, A, vol. 19, 1991, p. 465.
[42] Boerstoel H, Ypma M. WO 9606207 (Akzo Nobel).
[43] Meyer KH, Lotmar W. Helv Chim Acta 1936;19:68.
[44] Baule B, Kratky O, Treer R. Z Physik Chem (Leipzig) B 1941;50:255.
[45] Ingersoll HG. J Appl Phys 1946;17:924.
[46] Hermans PH. The physics and chemistry of cellulose fibres. Amsterdam: Elsevier, 1948.
[47] de Vries H. Appl Sci Res A 1952;3:111.
[48] Hermans PH, Kast W. Kolloid Z 1951;121:21.
[49] Kast W. Kolloid Z 1951;120:40.
[50] Kast W. Kolloid Z 1952;125:45.
[51] Kiessig H. Das Papier 1968;22:261.
[52] Ciferri A, Marsano E. Gazzetta Chimica Italiana 1987;117:567.
[53] Kroon-Batenburg LMJ, Kruiskamp PH, Vliegenhart JFG, Kroon J. J Phys Chem B 1997;101:8454.
[54] Northolt MG. Integrated fundamental polymer science technology, Elsevier applied science series, 1. Amsterdam: Elsievier, 1986. p. 567.
[55] Kroon-Batenburg LMJ, Northolt MG, Kroon J. Polym Commun 1986;27:290.
[56] Nishina T, Takano K, Nakame K. J Polym Sci B 1995;33:1647.
[57] Northolt MG, de Vries H. Die Angew Makromol Chem 1985;133:183.
[58] Northolt MG, van der Hout R. Polymer 1985;26:310.
[59] Northolt MG, Roos A, Kampschreur JH. J Polym Sci Part B Polym Phys 1989;27:1107.
[60] Baltussen JJM. Tensile deformation of polymer fibres. Thesis Technical University Delft, The Netherlands, ISBN 90-5651-027-4, 1996.
[61] Northolt MG, Baltussen JJM, Schaffers-Korff B. Polymer 1996;36:125.
[62] Baltussen JJM, Northolt MG. Polym Bull 1996;36:125.
[63] Hermans PH, Platzek P. Kolloid Z 1938;88:68.
[64] Gardner KH, Blackwell J. Biopolymers 1974;13:1975.
[65] Kroon-Batenburg LMJ, Kroon J. Carbohydrates in Europe 1995;12:15.
[66] Kroon-Batenburg LMJ, Bouma B, Kroon J. Macromolecules 1996;29:5695.
[67] Northolt MG. Eur Polym J 1974;10:799.
[68] Kazaryan LG, Tsvankin DY, Vasilev VA, Dakhis MA, Tolkachev YA. Polym Sci USSR 1975;17:1797.
[69] Kakida H, Chatani Y, Tadokoro H. J Polym Sci Phys Ed 1976;14:427.
[70] Kelly A. Strong solids. 2nd ed. Oxford, UK: Clarendon Press, 1973.
[71] Work RW. Text Res J 1949;19:381.
[72] Vos GJ, Koenders BM, Boerstoel H. WO 97/19207.
[73] de Vries H. Rayon revue, 1953. p. 173.
[74] de Vries H. Appl Sci Res 1952;A3:111.
[75] de Vries H. On the elastic and optical properties of cellulose fibres, Thesis, Technical University of Delft, 1953.
[76] de Vries H. Congres International de la Recherche Scientifique Appliqueé à l' Industrie Textile, Brussels, Belgium 1955.
[77] Sikkema DJ. In: Conference Proceedings of the Spring Joint Conference on Fibre Science, American Fibre Society, Mulhouse, France, 1997, p. 23.
[78] Klop EA, Lammers M. In: Conference Proceedings of the Spring Joint Conference on Fibre Science, American Fibre Society, Mulhouse, France, 1997, p. 26.
[79] Lammers M, Klop EA, Northolt MG. In: Conference Proceedings of the Spring Joint Conference on Fibre Science, American Fibre Society, Mulhouse, France, 1997, p. 28.
[80] Kolpak FJ, Blackwell J. Macromolecules 1976;9:273.